Journal of Applied Polymer Science

In vitro and *in vivo* investigational studies of a nanocomposite-hydrogel-based dressing with a silver-coated chitosan wafer for full-thickness skin wounds

Maneesh Jaiswal ,[1*] Veena Koul,[1] Amit Kr. Dinda[2]
Centre for Biomedical Engineering, Indian Institute of Technology, New Delhi, India 110016
Department of Pathology, All India Institute of Medical Sciences, New Delhi, India 110029
*Present address: Sumandeep Vidyapeeth Deemed University, Vadodara, Gujarat, India 391760
Correspondence to: M. Jaiswal (E-mail: jaiswal.maneesh@gmail.com)

ABSTRACT: A nanocomposite reservoir-type hydrogel dressing of poly vinyl alcohol (PVA) was fabricated by a freeze–thaw method and loaded with silver-nanoparticle-coated chitosan wafers (Ag–CHWs). The Ag–CHWs were synthesized by a sonication technique with silver nitrate ($AgNO_3$) and chitosan powder. Scanning electron microscopy images showed silver nanoparticles (AgNPs) with a size range of 10 ± 4 nm on the surface of the chitosan wafers, and the antibacterial efficacy (minimum inhibitory concentration) of the Ag–CHWs was measured against *Pseudomonas aeruginosa* (32 μg/mL), *Staphylococcus aureus*, (30 μg/mL) and *Escherichia coli* (32 μg/mL). The antimicrobial PVA hydrogel showed an improved tensile strength (~0.28 MPa) and gel content (~92%) in comparison with the blank hydrogels. Full-thickness-excision wound studies of the nanocomposite dressing on Wistar rats revealed enhanced wound contraction, improved inflammation response, re-epithelization rate, neoangiogenesis, and granulation tissue formation in comparison to the control group. A flexible, biocompatible, nanocomposite reservoir dressing not only established the chitosan as a stabilizer but also proved the efficacious and safe utility of AgNPs toward chronic wound management. © 2016 Wiley Periodicals, Inc. J. Appl. Polym. Sci. **2016**, *133*, 43472.

KEYWORDS: biocompatibility; biodegradable; biomaterials; degradation

Received 31 July 2015; accepted 21 January 2016
DOI: 10.1002/app.43472

INTRODUCTION

Since the pioneer work on hydrogels published by Wichterle and Lim in 1961,[1] a huge amount of attention has been given to its pharmaceutical and biomedical applications through the development of innovative medical devices. Because of their three-dimensional, soft, elastic, and tissue mimetic consistency, hydrogels have been proven to be a versatile formulation for drug-delivery, cell encapsulation, and tissue regeneration applications, particularly for wound-healing applications.[2–6] Their water absorption properties facilitate wound healing by preventing tissue dehydration and unwanted loss of vital nutrients from injured tissues. Moreover, the hydrated environment accelerates angiogenesis and the breakdown of dead tissue and fibrin and enhance the interactions of growth factors with their target cells. Despite having all favorable features, hydrogel dressings support fungal infections and bacterial colonization in the wound bed because of their moist environment. Conventional antibiotic therapies include the release of active constituents from the dressing into the wound milieu. The healing applications of these therapies have been limited because of microbial resistance and systemic side effects, which hamper the activities of growth factors and cytokines and cause subsequent damage to the growing tissues.[7–10]

Colloidal silver nanoparticles (AgNPs) are unique and very effective broad-spectrum antiseptics against variety of aerobes, anaerobes, yeast, fungi, and viruses. Widgerow[11] demonstrated their direct impression on healing promotion by way of a reduction in cytokine-modulated inflammation, that is, neutrophils apoptosis through the augmentation of the activities of matrix metalloproteinases and negative modulation of the transforming growth factor β. AgNPs have been proven to be an indispensable tool of nanotechnology for modern wound management.[12–14] In particular, because of their broad-spectrum antimicrobial activity, chemical stability, and economy, AgNPs have been investigated extensively for antiseptic wound dressings and are available as Acticoat, Arglaes, Aquacel-Ag,

Additional Supporting Information may be found in the online version of this article

Silvasorb, Actisorb, Silver-200, and Urgo-Tul SSD.[12,15–17] However, researchers have controversial views on the safety aspects of silver dressings in clinical applications. The availability of silver ions in the wound bed to maintain a continual aseptic environment throughout therapy is the key element required for an ideal wound dressing. Tian *et al.*,[18] mentioned the positive effects of Ag NPs on wound healing because of their antimicrobial properties and modulating effect on fibrogenic cytokines and inflammatory mediators. A number of composite products have been developed to incorporate AgNPs in the form of thin films, hydrogels, sol–gels, porous polymers, AgNP-doped biocompatible polymers, and viscous resins.[12–14,17] Many researchers have used synthetic polymeric hydrogels (viz. poly (acryl) amide and poly vinyl alcohol) as wound-dressing materials, but none of them have mentioned the safety aspect of these hydrogel composites.[19,20] Chitosan, a natural polysaccharide, composed of *N*-glucosamine and *N*-acetyl glucosamine units, possesses inherent antimicrobial, hemostatic, and wound-healing properties and acts as a stabilizer for AgNPs.[21] It has stimulating properties toward phagocytes and promotes the regeneration of connective tissues, angiogenesis, and the production of fibroblasts, cytokines, and growth factors. It has been found to be an interesting biomaterial for tissue engineering, particularly for wound-healing applications.[21–23]

With consideration of the previous facts, we designed and synthesized a nanocomposite-hydrogel-based antimicrobial-reservoir dressing for chronic wound-healing applications. Silver-nanoparticle-coated chitosan wafers (Ag–CHWs) were synthesized by a sonication technique. Ag–CHW-loaded PVA hydrogels were formulated by physical crosslinking (with the freeze–thaw method). PVA was selected for hydrogel preparation because of its versatile properties, that is, its water solubility and biocompatibility (U.S. Food and Drug Administration approved), and because it has been explored for various biomedical applications, such as drug delivery, cell encapsulation, wound healing, and tissue engineering.

Many physical and chemical crosslinking techniques have been used by researchers to prepare PVA hydrogels; these techniques include chemical crosslinking by glutaraldehyde, bisacrylamide, boric acid, epichlorohydrin, acid chloride, and dicarboxylic acid and physical crosslinking by the freeze–thaw method and ionization-based γ irradiation or photocrosslinking.[24–27] The freeze–thaw method has been the most convenient and is an effective technique for the preparation of PVA hydrogels with high water-retention capacities.

In this research work, the extensive investigation of AgNPs, their incorporation into PVA hydrogels, and physicochemical and microbiological studies of dressings were performed by means of various physicochemical tools. The biocompatibility aspect and wound-healing assessment of nanocomposite PVA hydrogels were studied with a full-thickness excision wound model.

EXPERIMENTAL

Materials

PVA (molecular weight $\approx$ 125,000, degree of hydrolysis $\approx$ 98%) and chitosan (degree of deacetylation $\geq$ 95%) were purchased from Sigma-Aldrich. $AgNO_3$ was purchased from Spectrochem Pvt., Ltd. (Mumbai, India), and isopropyl alcohol (IPA) was purchased from Qualizen India Pvt., Ltd. Sterile Petri dishes (15 mm) were purchased from Tarson Pvt., Ltd. (India). Luria agar and Luria broth media were purchased from Hi-Media India Pvt., Ltd. *Pseudomonas aeruginosa* (PA), *Escherichia coli* (EC), and *Staphylococcus aureus* (SA) strains were procured from the Department of Biochemical & Biotechnology of the Indian Institute of Technology.

Synthesis of the Ag–CHWs by the Sonication Method

Ag–CHWs were synthesized by a sonication method as reported by Okitsu *et al.*[28] with a little modification. Briefly, a 1.0% w/v aqueous suspension of chitosan was purged with N_2 for 15 min and then 10% v/v IPA and 0.5 m*M* $AgNO_3$ were added in ascending order. The whole suspension was immediately sonicated by means of a sonication probe (Hielscher-UP200S, Germany) for 10 ± 1 min at a high amplitude and 100% sonication cycles. As sonication progressed, the transparent suspension turned from yellow to light gray. The insoluble chitosan flakes were found suspended in the aqueous media. After the completion of the sonication procedure, the Ag–CHW suspension was centrifuged and washed with distilled water. The lyophilized dried samples were characterized by morphological and surface examinations.

Characterization of the Nanoparticles

Morphological Assessment. The size, morphology, and adsorption of the AgNPs on the chitosan surfaces and their distribution were assessed by scanning electron microscopy (SEM) and transmission electron microscopy (TEM). For the SEM images, the lyophilized Ag–CHW was coated with gold by a sputter coater, and the images were captured at 70,000 $\times$ magnification. For the TEM micrographs, the lyophilized Ag–CHWs were resuspended in distilled water and sonicated again for 1 min to disaggregate the suspension, and a drop of this solution was placed onto a copper grid and observed at random places to determine the nanoparticle sizes.

X-ray Diffraction (XRD) Study. The powder XRD patterns of the pure chitosan powder and Ag–CHWs were recorded with an XRD instrument (XRD-PW 1700, Philips) at 19 °C with Cu Kα radiation generated at 40 kV and 40 mA. The range of diffraction angles (2θs) was 10–80°. The scan speed was 2.5 °/min, and a graphite filter was used during continuous-scan mode.

Minimum Inhibitory Concentration (MIC). The antibacterial efficacy of the Ag–CHWs was evaluated as the MIC value against Gram-positive (PA and SA) and Gram-negative (EC) bacterial strains with the agar-plate, colony-counting method.[4] The MIC values of the Ag–CHWs were determined with eight different concentrations (10, 15, 20, 25, 30, 40, 50, and 100 µg/mL). Sterile Luria agar (15 mL) plus a predetermined concentration of Ag–CHW solution were poured into a sterile plastic plate and allowed to solidify under a laminar hood. A volume of 100 µL of bacterial culture was spread uniformly on the solidified media, and the plates were placed in an incubator at 32 ± 0.2 °C for 24 h. The quantity of bacterial inoculum required to get 300–400 bacterial colonies in the control plates was optimized before the experiments by serial dilution. The

number of growing colonies were counted with a colony counter. The concentration of the Ag–CHWs in which no colony appeared was considered to be the MIC of the Ag–CHWs for that particular bacterial species. The experiment was repeated three times with five dishes at each concentration (for each bacterial species).

Preparation of the PVA Hydrogels by the Freeze–Thaw Method

Antimicrobial hydrogel dressings containing Ag–CHWs were prepared by the freeze–thaw method.[24,25] The required amount of Ag–CHWs (150–160 μg/dressing, as determined by MIC) was added to a 12% w/v aqueous PVA solution and stirred overnight to produce a homogeneous solution. This was poured into sterile glass Petri dishes under laminar flow and sealed with Parafilm. Thereafter, these plates were treated with repetitive freeze–thaw cycles for the preparation of the PVA hydrogel according to Hassan *et al.*[25] with little modifications. Briefly, they were frozen for 16 h at −20 °C; this was followed by thawing at 10 °C for 2 h in the first cycle. During the next cycles, freezing was carried out for the same time duration, whereas the thawing period was increased from 2 to 6 h. The cycles were repeated six times, and the samples were stored at −20 °C until further characterization was carried out.

Characterization of the Hydrogels

SEM. For the surface morphological studies, hydrogels discs (8 mm in diameter) were sliced at its equilibrium swelling state with a biopsy punch and lyophilized at −80 °C. SEM images were captured from randomly selected areas after gold coating with a vacuum sputter coater (EMI TECK, K550X; Carl Zeiss, Thornwood, NY) at a 0.09-mbar vacuum pressure.

Tensile Testing. For the determination of the effects of the Ag–CHWs on the elasticity and tensile strength of the hydrogel dressing, dumbbell-shaped specimens were made with a metallic cutter as per ASTM-D-638 (gauze length = 6 cm, width = 0.8 cm, thickness = 0.3 cm) and placed between two metallic vertical toothed grips of a uniaxial tensile testing machine (Tinius Olsen, Q4368, H5KS, Q-Mat 5.37 software).[26,27] The Young's modulus and maximum elongation at break of the hydrogel samples were observed in their equilibrium swelling state. The experiment was performed at a 9.0 mm/min extension rate and 100-kN maximum load under controlled humidity (65 ± 3%) and temperature (25 °C). To remove any chances of deformation, the samples were stretched twofold up to half of their grip length.

Equilibrium Swelling Ratio and Gel Content. The water-uptake capacity of the PVA hydrogel and Ag–CHW-loaded PVA hydrogels equilibrium were evaluated by the immersion of about 20-mg circular discs (0.5 cm in diameter) in distilled water at 37 °C for 24 h at 75 rpm in an incubator shaker.[28] The sample discs were wiped with tissue paper and weighed. The difference in weight after and before swelling were used to calculate the equilibrium swelling ratio as per the following formula:

$$\text{Equilibrium swelling ratio}(\%) = (W_t - W_i / W_i) \times 100 \quad (1)$$

where W_i is the initial weight of the dry hydrogel sample and W_t is the weight of the hydrogel at time t.

For the gel content measurement, the swollen hydrogel discs were again dried to a constant weight, and the percentage conversion was evaluated by the following formula:

$$\text{Gel content}(\%) = (W_d / W_t) \times 100 \quad (2)$$

where W_d is the initial weight of the dry hydrogel sample and W_t is the dry weight of the hydrogel at time t (after incubation in distilled water for time t).

Silver Content Estimation by Energy-Dispersive X-ray (EDX) Spectroscopy

The quantitative analysis of silver in the Ag–CHW-loaded PVA hydrogel was performed with a field emission scanning electron microscope equipped with EDX spectroscopy. Two types of specimens were prepared: (1) a hydrogel at time 0 (before the silver-release study) and (2) a hydrogel after the silver-release study in phosphate-buffered saline (PBS; pH 6.5) at 35 °C for 5 days. As EDX is a surface analysis technique only and results from the penetration of the beam to the micrometer-level depth from the surface, the selected specimens were lyophilized and crushed to powder before we measured the silver content. The carbon-coated specimens were randomly analyzed with a 20-kV energy source from five different positions of the lyophilized specimen.

Antimicrobial Activities of the Ag–CHW-Loaded Hydrogels

The antimicrobial activities of the Ag–CHW-loaded PVA hydrogels were evaluated according to the U.S. Clinical and Laboratory Standards Institute disc-diffusion method.[3] An amount of 1×10^5 colony-forming units of the test strain (EC) was spread on a solid agar plate under aseptic conditions. Ag–CHW-loaded PVA hydrogel discs 8 mm in diameter were cut with a biopsy metal punch and placed on that surface. The control disc was dipped in a 1% tetracycline (TC) solution and placed in the same way on the same Petri dish. After 48 h of incubation at 32 °C, the zone of inhibition (because of the release of the AgNPs) was measured.

In Vivo Wound-Healing Experimentation

Experimental Protocol. The effects of the silver–chitosan nanoparticulate system on skin tissues in terms of inflammatory response and the healing efficacy of a moist dressing (PVA hydrogel) on full-thickness excision wound healing were evaluated with male Wistar rats as an animal model. Rats approximately 180 ± 20 g in body weight were selected. The whole experiment was performed according to the ethical approval and guidelines of the All India Institute of Medical Sciences (362/IAEC, AIIMS, New Delhi, India). The animals were divided into three groups: (1) cotton gauze (control), (2) PVA hydrogel dressing (denoted as PVA), and (3) antimicrobial nanocomposite PVA dressing (denoted as PVA/Ag–CHW). In each group, 12 rats were taken. Each group was subdivided in two groups: group A (6 rats) for wound-contraction rate and histological evaluation on day 3 and group B (6 rats) for the same parameters on day 8.

Full-Thickness Excision Wound Model. Male Wistar rats were anaesthetized with an Intra-muscular injection of 100 µL of a 0.5% w/v Ketamine solution (Keta). From the dorsal side of the rat, hairs were shaved with an electric hair clipper (Moser, Germany) and wiped with 70% v/v ethanol. A full-thickness excision wound (up to the depth of the loose subcutaneous layer) with a diameter of 2.0 cm was created with a sterile surgical scalpel blade and scissors on the shaved zone and wiped with sterilized saline before the application of the dressing.[29]

After the wound was created, a dressing was applied on the control and the treated group. In the control animal group, the wound was covered with sterile cotton gauze (soaked with saline), and the Ag–CHW-loaded PVA hydrogel and the PVA blank hydrogel were applied in the equilibrium swelling state and covered with a cellophane membrane. To keep the dressing in its proper position, the hydrogel was covered with microporous adhesive tape. On days 3 and 8, the animals were sacrificed, and skin tissue from the wound area was collected.

Prohealing Parameters. We measured wound contraction planimetrically on days 0, 3, and 8 by marking the edges of the healed boundary with a marker on transparent tracer paper, and the comparative healing rate was studied by means of the average wound contraction in comparison to the control group.[30–32] The percentage (%) wound contraction was calculated with the following equation:

$$\%\,\text{Wound contraction} = (A_i - A_t / A_i \times 100) \quad (3)$$

where A_i is the initial wound area at day 0 and A_t is the area of the wound at time t.

Histological Examination. For the measurement of the histopathological aspects and for wound-contraction assessment, the wound tissues were collected after the sacrifice of the animals on days 3 and 8. The wound tissues with its peripheral zone were fixed with 10% formalin, embedded in paraffin, and sectioned (3.0 µm) with a microtome (RM2235, Leica, Germany). The hematoxylin and eosin (H&E)-stained sections were examined under a light microscope independently by two individuals for the semiquantitative grading of different parameters for the assessment of the healing process (acute/chronic inflammation, fibrosis, number of fibroblast cells, neovasculature, and collagen fibrils).[13] All morphometric parameters were recorded with an image analyzer (Olympus microscope BX61, Japan) with an image-analyzing computer program (Image-Pro Plus 6.3, Media Cybernetics). The epidermis and dermal regions were evaluated. A minimum of 50 high-power fields (hpfs; 40×) were assessed. Six hpfs from each one of the six animals were selected for the grading, and an average was considered for data evaluation. Acute inflammation was graded by the average number of acute inflammatory cells (neutrophil)/hpf: less than 1/hpf (grade ±), 1–2/hpf (grade +), 3–4/hpf (grade ++), 5–6/hpf (grade +++), and more than 6/hpf (grade ++++). Similar grading was followed for chronic inflammation through the assessment of the number of chronic inflammatory cells (lymphocytes, histocytes, and plasma cells) per hpf. We assessed the degree of edema by noting the intercellular space in the upper dermis. Edema was graded as ± if the loose space was seen in less than 5 out of 50 hpf, + in 5–10 hpf, ++ in 11–20 hpf, +++ in more than 20 hpf. The granulation tissue consisted of plump fibroblasts with large vesicular nuclei, which represented proliferating fibroblasts. It was graded as + with less than 25 such cells/hpf, ++ with 26–50 cells/hpf, and +++ with greater than 50 cells/hpf. With maturation, these immature plump fibroblasts became mature fibroblasts with spindle-shaped nuclei and eosinophilic abundant cytoplasm, which represented collagenization. With extracellular collagen deposition, the number of mature fibroblasts decreased per hpf with increasing intercellular eosinophilic hyaline material. When such material was seen in less than 25 out of 50 hpf, the collagen deposition was graded as +, and when it was seen in 25 or more hpf, it was graded as ++. We assessed angiogenesis by counting the number of capillaries in the upper dermis. We graded them as less than 5/hpf (±), 5–10/hpf (+), and more than 10/hpf (++). The re-epithelialization was evaluated by the assessment of the regenerating epidermis. It was graded as ± if it had less than two cell layers, as + if it had two to three cell layers, as ++ if it had three to four cell layers, and +++ if it had five or more cell layers. All histological sections were assessed in ascending order through the center of the wounds to obtain the maximum wound diameter.[24,29]

Statistical Analysis

Data are expressed as the means and standard deviations, and the statistical significance between the experimental and control values was analyzed by analysis of variance followed by Dunnett's test with Graph Pad Prism 2.01 (Graph Pad Software, Inc., La Jolla, CA). A p value of less than 0.05 was considered statistically significant.

RESULTS AND DISCUSSION

The wound-healing process is often delayed by a dry wound environment and bacterial infestation at the site; this eventually suppresses the skin regenerative process. The antibacterial effects of silver in biocompatible polymeric matrix are required for a longer duration without its leaching in the wound bed, as it has reported to illicitly darken the skin (this is also known as *argyria*) and delayed wound healing because of its reactions in biological fluids.[25] Apart from the detrimental effect on the wound tissues, the AgNPs also exhibited concentration-dependent systemic toxicity to vital body organs (i.e., liver and renal dysfunction).[9,10,33] Tian *et al.*[18] mentioned that AgNPs reduced scar appearance in a dose-dependent manner and also decreased inflammation through cytokine modulation. In this study, an attempt was made to overcome a few critical issues related to dressing materials for nonhealing chronic wounds through the design and development of a hydrogel-based nonadherant, hydrated, elastic, and antimicrobial-reservoir dressing. The antimicrobial and antifungal properties were imbibed by the *in situ* incorporation of colloidal silver-coated chitosan wafers into PVA hydrogel dressings.

Synthesis of the Ag–CHWs

AgNPs were successfully synthesized by a sonication technique, which involved the formation of high-energy cavitation bubbles. High-speed sonication generated a fine suspension of silver-adsorbed chitosan (Ag–CHW) that mixed quite easily with the PVA solution. Under typical experimental conditions (chitosan/$AgNO_3$ ratio = 2:1 w/w with 10% v/v IPA in ascending order and 10 ± 1 min of sonication time), the Ag–CHWs were formed

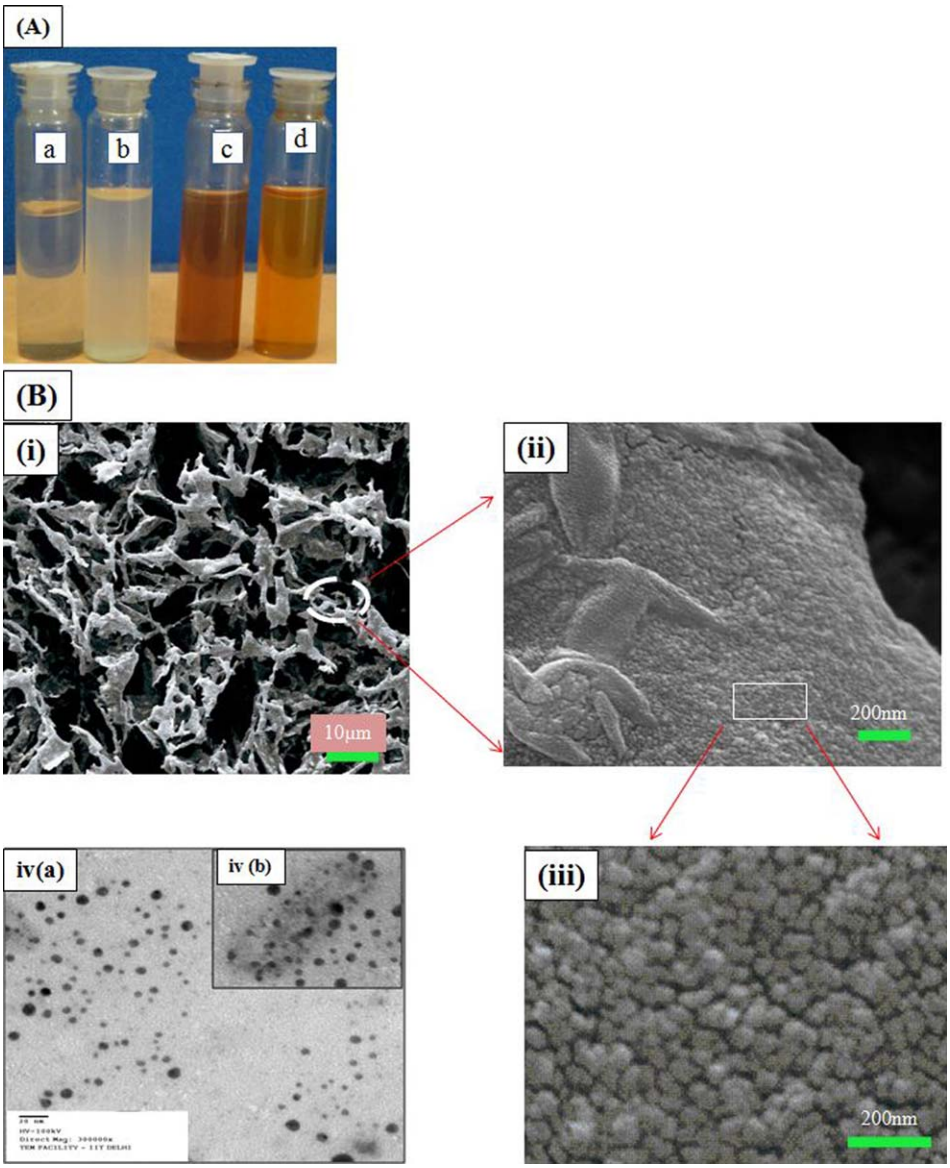

Figure 1. (A) Sonication products of (a) an $AgNO_3$ solution (0.02 mol), (b) a chitosan solution (0.02%), (c) $AgNO_3$/chitosan (1:1 w/w), and (d) $AgNO_3$/chitosan (2:1 w/w). (B) SEM images of silver–chitosan nanoparticles (Ag–CHWs) at various magnifications [(i) 1000, (ii) 40,000, and (iii) 70,000×] and TEM images of [iv(a)] silver–chitosan nanoparticles at a magnification of ×30,000 and [iv(b)] AgNPs adsorbed onto a chitosan fragment. The bar indicates 20 nm. [Color figure can be viewed in the online issue, which is available at wileyonlinelibrary.com.]

[Figure 1(A)]. The whole process involved radical formation and pressure because of the generation of cavitational bubbles. The reaction of a sonication process was carried out in the following steps as per Okitsu *et al.*[28]:

$$H_2O \xrightarrow{\text{Sonication}} .OH + H$$

$$IPA + .OH(H) \rightarrow (CH_3)_2{}^{\cdot}COH + H_2O(H_2)$$

$$IPA \xrightarrow{\text{Pyrolysis}} \text{Pyrolysis products}$$

$$Ag^n + \text{Reducing Species} \rightarrow Ag^{(n-1)} + R^{\cdot} + H^+$$

$$nAg^0 \rightarrow (Ag^0)$$

where the symbol · indicates ultrasonic irradiation. In the first step, the pyrolysis of water took place with the formation of the .OH/.H radical. In the second step, dimethyl ketyl radicals were formed via the reaction of IPA with radicals. During sonication, IPA was converted to a reducing species, which further reduced Ag^+ to form AgNPs.

Characterization of the Ag–CHWs

Morphological Assessment. SEM images of the Ag–CHWs are shown in Figure 1[B(i–iii)]. We observed that the AgNPs were distributed all over the chitosan flakes. Chitosan acted as a natural stabilizer for the colloidal AgNPs. It was added to the reaction mixture just before the sonication step so that silver ions (Ag^+) were reduced before attachment to the surface. Because of the aggregation of nanoparticles, slightly larger sized particles are shown in the SEM images, but their actual size (disaggregated) is shown in the TEM images. The particles were either

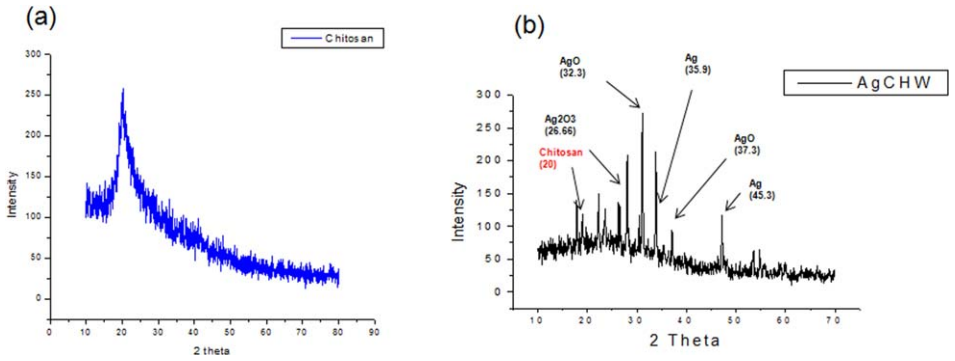

Figure 2. XRD spectra of (a) pure chitosan powder and (b) Ag–CHWs, which indicate AgNPs (Ag), Ag_2O, and Ag_2O_3. [Color figure can be viewed in the online issue, which is available at wileyonlinelibrary.com.]

an agglomerate of many crystallites or a single grain/crystallite. In our study, many AgNPs aggregated onto the chitosan wafer during sample preparation (i.e., drying over the glass cover slip), whereas in TEM, each flake of chitosan was observed to have plenty of separated AgNPs with sizes of nearly 10 ± 4 nm, as demonstrated in Figure 1[B(iv)].

XRD Analysis of the Ag–CHWs

XRD patterns were used to define the crystallographic pattern and atomic composition of the sample material by the position and intensity maxima. Figure 2(a,b) shows the crystalline form of chitosan and the Ag–CHWs, respectively. A sharp diffraction peak at 20° [Figure 2(a)] indicated the characteristic peak of chitosan flecks, whereas the Ag–CHWs [Figure 2(b)] showed multiple peaks, assigned to AgNPs (35.9 and 45.3°), silver oxide (Ag_2O; 32.57°) and silver trioxides (Ag_2O_3; 32.63°, according to International Centre for Diffraction Data, 1998). The XRD patterns of the nanoparticles indicated a certain degree of interaction in which chitosan and the Ag–CHWs were observed along with some impurity peaks of silver oxides; these indicated the formation of the Ag–CHW nanocomposite.

Antimicrobial Activity. Nonhealing wounds often undergo bacterial manifestation and contribute chiefly to mortality, especially in the case of third-degree burns. AgNPs have proven to be active against most bacterial and fungal species, but their safe and controlled delivery are critically important; otherwise, they adversely affect the progression of the healing cascade. SA, EC, and PA are the main bacterial strains found in the wound environment and need immediate control for the progression of the healing process. Therefore, the MICs of the silver–chitosan nanocomposite (Ag–CHWs) was investigated against SA, EC, and PA and were found to be 30, 32, and 32 μg/mL, respectively [Figure 3(A)]. The MIC was also needed to ascertain the minimum quantity of the Ag–CHWs required to be incorporated in the hydrogel patch according to its volume to form an effective wound covering without causing an overdose of AgNPs.

Synthesis of the Antimicrobial PVA Hydrogel by the Freeze–Thaw Method

The calculated amount of Ag–CHWs were incorporated *in situ* in the PVA solution before we proceeded with the freeze–thaw steps. When the PVA solution underwent repeated freeze–thaw cycles, the hydrogel was formed by means of three possible mechanisms: (1) direct hydrogen bonding, (2) direct crystallite formation, and (3) liquid–liquid phase separation followed by a gelation mechanism. Hydrogen bonding led to nodes and crystallite formation; this resulted further in the formation of larger polymeric crystals. During the freezing process, the system underwent spinodal decomposition, whereby polymer-rich and polymer-poor phases appeared spontaneously in the homogeneous solution followed by a gelation process; this resulted in more distantly spaced crosslinks.[34] We assumed that phase separation through spinodal decomposition could have been responsible for the improved mechanical strength of the crosslinked PVA network, which formed by a mechanism of polymer quenching.[35]

Characterization of the Nanocomposite Hydrogel (PVA/Ag–CHW)

SEM. As shown in Figure 4(B,D), the PVA-coated Ag–CHWs were observed on the surface and in the depth of the hydrogels (marked with arrows). The pore size is another very crucial property of porous hydrogels; it influences the water-absorption capacity and is governed by the density of the crosslinking network. As shown in Figure 4(A,C), the surface and internal morphologies of the nanocomposite hydrogel dressing were observed. An interconnected porous internal architecture with pore sizes in the range of 10–15 μm was noted from lyophilization; these were developed during the swelling and lyophilization process. Such a morphology protect the wound from microbial penetration across the dressing and also offers a long-lasting aseptic environment in the healing area. Additionally, the pore size and their orientation also influence the cell-proliferation potential of the scaffolds; interconnected pores allow the growing cells to connect with the surface and offer a space for their migration.[36]

Swelling Properties. The swelling profiles of the PVA hydrogel and nanocomposite PVA hydrogels in PBS were studied at 37 °C. The equilibrium swelling ratio was found to be about 651 and 604%, respectively, in PBS (pH 6.5) at 37 °C (Table I). The findings of the swelling data indicated that the presence of the Ag–CHWs did not have significant adverse impact on the swelling capacities of the matrixes as an indicator of the least hindrance of the AgNPs for media transport. The only factor involved in the swelling behavior was the presence of functional groups of PVA (—OH) and chitosan (—OH, —NH_2). These

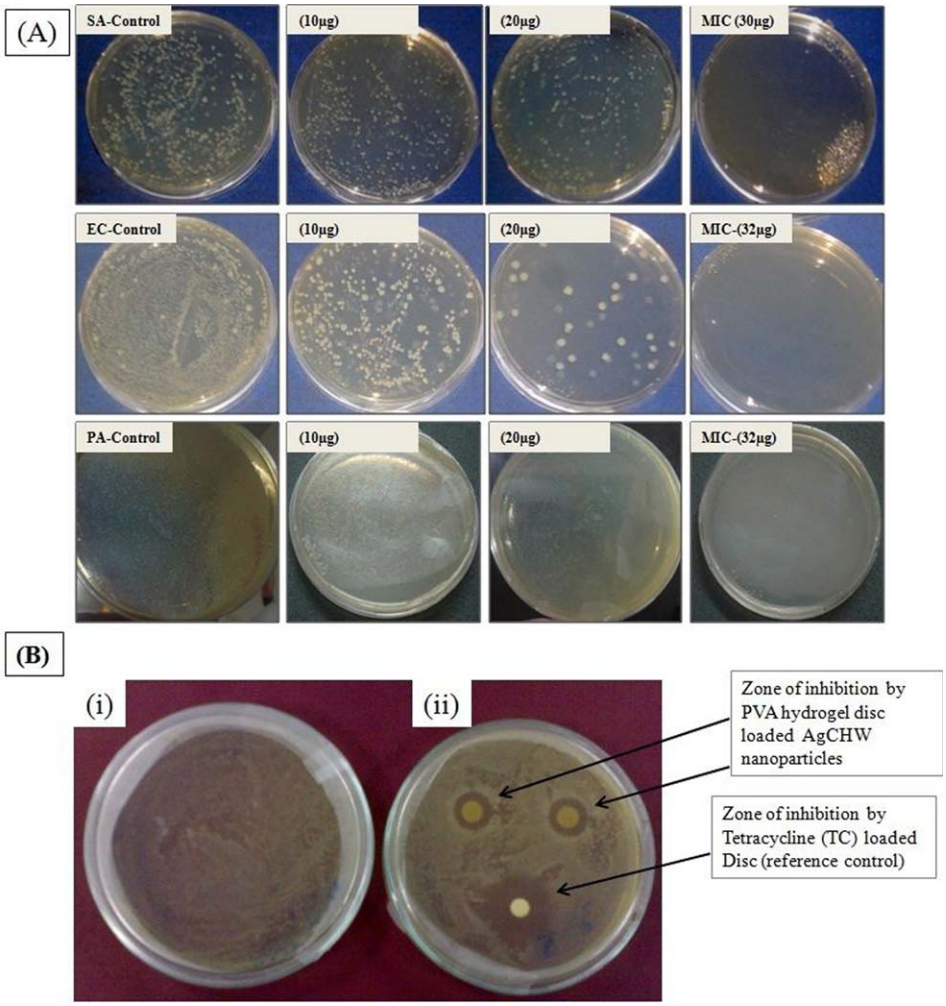

Figure 3. (A) Optical images of culture plates with agar media demonstrating the antimicrobial activity of Ag–CHW nanoparticles against EC, PA, and SA. (B) Zone of inhibition (antimicrobial activity) of (i) Ag–CHW-loaded PVA hydrogels and (ii) TC-loaded discs. [Color figure can be viewed in the online issue, which is available at wileyonlinelibrary.com.]

groups influenced the swelling pattern by way of ionization in the buffer media and also by hydrogen bonding with water molecules.[27] After ionization, the repulsive forces of these groups propelled each other; this led to the swelling of the crosslinked hydrogel networks, whereas neutral groups contributed to water uptake by participating in hydrogen bonding with water molecules.[29]

The gel contents of the PVA and nanocomposite PVA hydrogels were found in the range 90–92%; this indicated the applicability of an effective crosslinking method for hydrogel preparation. The water loss in first-degree burn wounds was 20 times higher ($5138 \pm 202\ g^2$/day) in comparison to normal injuries ($279 \pm 26\ g^2$/day). Therefore, a high water-retention capacity of a hydrogel dressing will retain the moist environment in the vicinity of the wound and, thereby, help in the formation of granulation tissues.[37]

Mechanical Properties of the Hydrogels. Figure 5(B) shows the force (N) versus displacement (mm) curve of the hydrogel specimens [PVA blank and PVA/Ag–CHW hydrogel; Figure 5(A)]. The data of the mechanical properties are tabulated in Table I. From the result, we observed that the maximum elongation and tensile strength increased by about 95 and 30%, whereas the Young's modulus also increased by fivefold with the inclusion of the Ag–CHWs in the PVA hydrogel. With the inclusion of the nanoparticles, the distance between the two physically crosslinked PVA chains might have increased, and this resulted in an improved elasticity. Moreover, the silver–chitosan nanoparticles interacted with the PVA chains by physical means; this made the polymeric chains become highly immobilized.[38,39] An additional possible bonding between the Ag–PVA molecules (i.e., Ag—OH bonds) was simulated through sigma coordination by the donation of an oxygen electron lone pair to silver, which could have participated in the high stiffness and increased the tensile strength of the nanocomposite hydrogel in comparison to the PVA hydrogel. An increase in the tensile strength with the addition of the Ag–CHWs may also have been supported by the study performed by Lee *et al.*[40] on a poly (ethylene) glycol hydrogel network. A higher tensile strength (0.279 MPa) and Young's modulus (0.65 Psi) are important features for wound-dressing materials for maintaining the protective barrier for desired time periods.

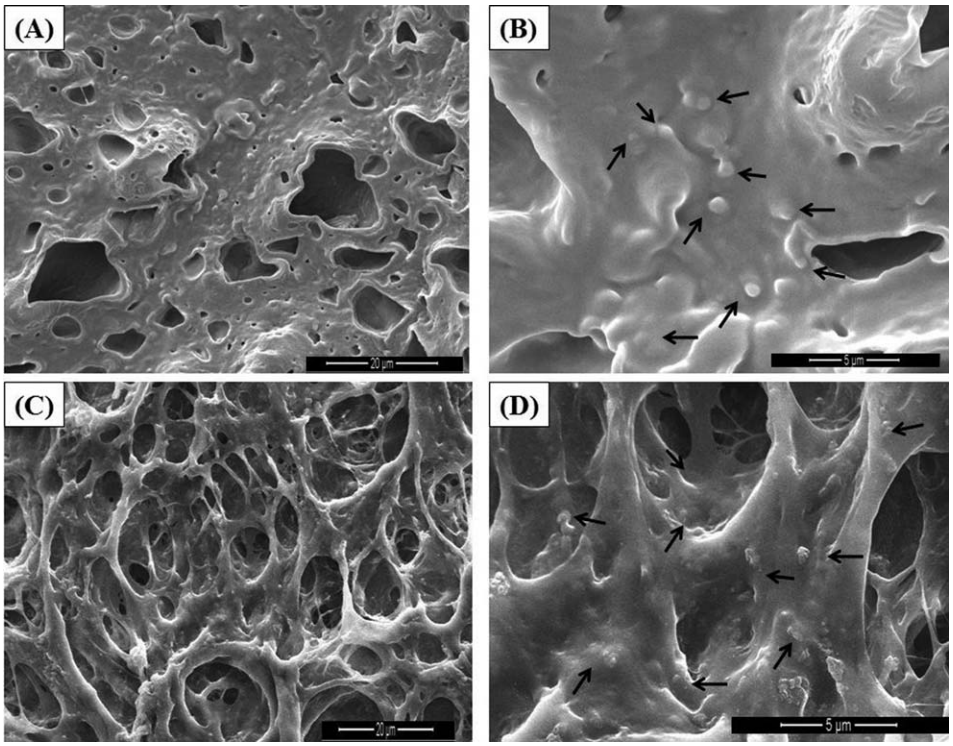

Figure 4. SEM micrographs showing the morphology of a PVA/Ag–CHW hydrogel (A,B) from the surface and (C,D) in-depth [(A,C) 5000 × magnification and (B,D) 15,000 × magnification].

Elemental Analysis of the Nanocomposite PVA Hydrogel by EDX Spectroscopy

The safe, effective, and long-term application of AgNPs are a primary requirement of wound-dressing materials because of their toxicity-related issues on normal cells. From the viewpoint of these aspects, reservoir-based nanocomposite dressings were evaluated for silver content after 5 days of incubation in a buffer medium. EDX provides a qualitative and quantitative elemental analysis of the matrixes.[41] Figure 1 in the Supporting Information presents the elemental spectrum from a randomly selected area of a PVA/Ag–CHW hydrogel specimen before and after silver release in PBS (pH 6.5), respectively (also mentioned in Table I in the Supporting Information). We noticed that the PVA hydrogels initially contained about 8.26% silver, 50% carbon, and 40% oxygen. Traces of sulfur and chloride were also present. The silver content was reduced from about 8.26 to 7.89% after 5 days of incubation in PBS (pH 6.5). It was interesting that only 4.47% silver was released from the matrixes; this indicated that silver remained in the hydrogels and not in the wound tissue, which could have otherwise initiated unwanted effects on growing tissues. The results were also signified the ability of chitosan to act as a stabilizer for the AgNPs.

Antimicrobial Activity

AgNPs are broad-spectrum antimicrobials, and they have efficacy against drug-resistant pathogens of clinical importance. The antimicrobial activity of the PVA hydrogels were evaluated by an agar-plate, disc-diffusion method against EC (a Gram-negative bacteria). Silver-loaded PVA discs were placed on a bacterial cultured plate. TC-loaded sterile discs were used as a control. The clear zone of inhibition was observed in both the TC-loaded sterile discs and nanocomposite PVA discs [Figure 3(B)]. We observed that the zone of inhibition was significantly less ($p < 0.05$) in the case of the nanocomposite discs. We inferred that the Ag–CHWs were embedded in the PVA hydrogel matrixes and acted as a reservoir in the dressing. The novelty of these reservoirs offered two added advantages. First, the lower quantity of AgNPs (4.47%) did not elicit any adverse effect on the nascent tissues (discussed in the next section); second, about 95% silver remained in the matrix as a reservoir,

Table I. Effects of the Ag–CHWs on the Mechanical Properties and Water-Uptake Properties of the PVA Hydrogel ($n = 5$)

Hydrogel	Maximum elongation (%)	Tensile strength (MPa)	Elastic modulus at maximum tensile strength (PSI)	Water-uptake capacity (% of dry weight of the hydrogel)
PVA hydrogel	125 ± 4%	0.214 ± 0.04	0.11 ± 0.2	651
Nanocomposite PVA hydrogel	244 ± 7%	0.279 ± 0.06	0.62 ± 0.13	604

The data are presented as means and standard deviations.

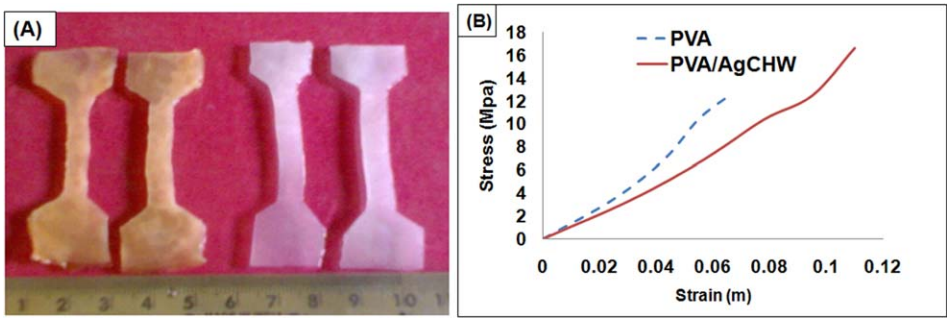

Figure 5. (A) Hydrogel specimens for tensile testing and (B) stress–strain curves of the PVA hydrogel and Ag–CHW-loaded PVA hydrogel. [Color figure can be viewed in the online issue, which is available at wileyonlinelibrary.com.]

and we hypothesized that this reservoir could function as a long-lasting antimicrobial scaffold.[9,33]

In Vivo Biocompatibility and Wound-Healing Studies

Tissue compatibility is an important and necessary requisite of the dressing; this ensures its safe application. Such properties of nanocomposite hydrogel dressings were investigated by their application on full-thickness excision wounds on Wistar rats. The PVA hydrogel and cotton gauze were selected as control groups. On days 3 and 8, the wound-contraction rate and histological evaluation were carried out to observe the inflammatory response and rate of re-epithelization and other prohealing parameters. The results of these parameters are shown in Figures 6 and 7.

Wound Contraction. The wound-contraction data of the healing progression with respect to time was provided by the planimetric method. On day 8, the nanocomposite hydrogel dressing showed a significantly higher ($p < 0.05$) contraction of the wound area ($1.63 \pm 0.5\,cm^2$, 48%) in comparison to the cotton

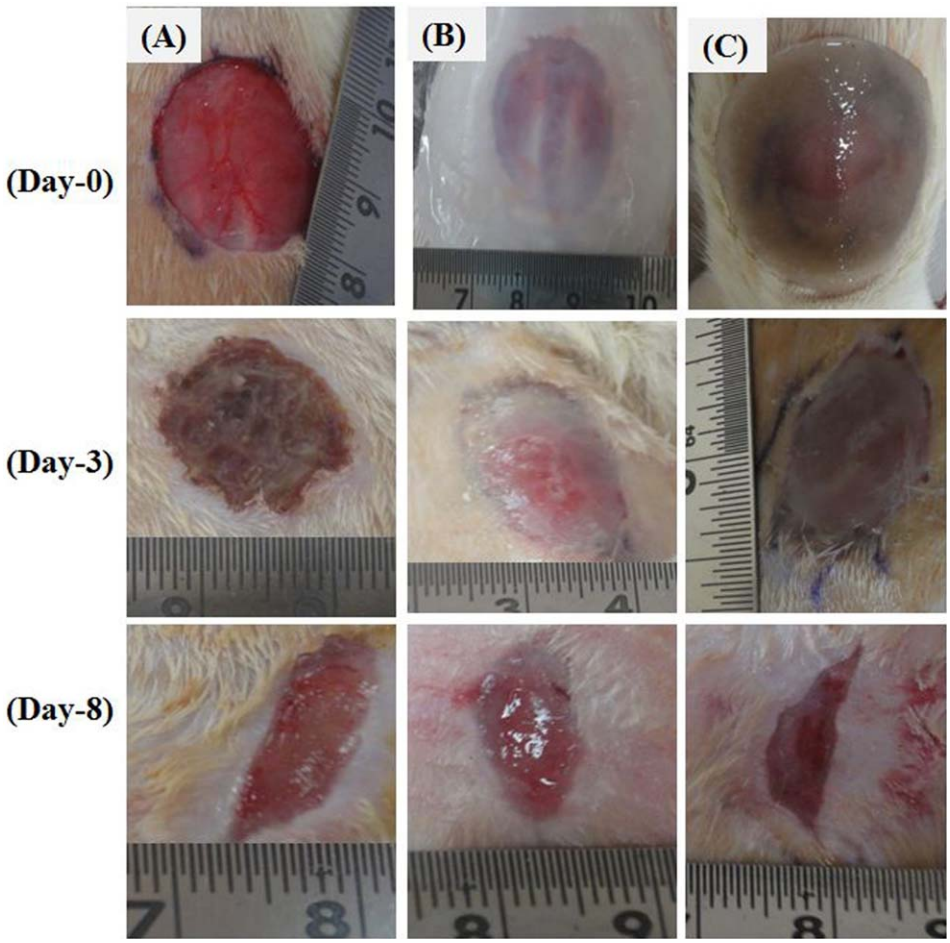

Figure 6. Optical images of an excision wound on days 0, 3, and 8 treated with (A) cotton gauze, (B) the PVA hydrogel, and (C) the nanocomposite antimicrobial hydrogel dressing (PVA/Ag–CHW). [Color figure can be viewed in the online issue, which is available at wileyonlinelibrary.com.]

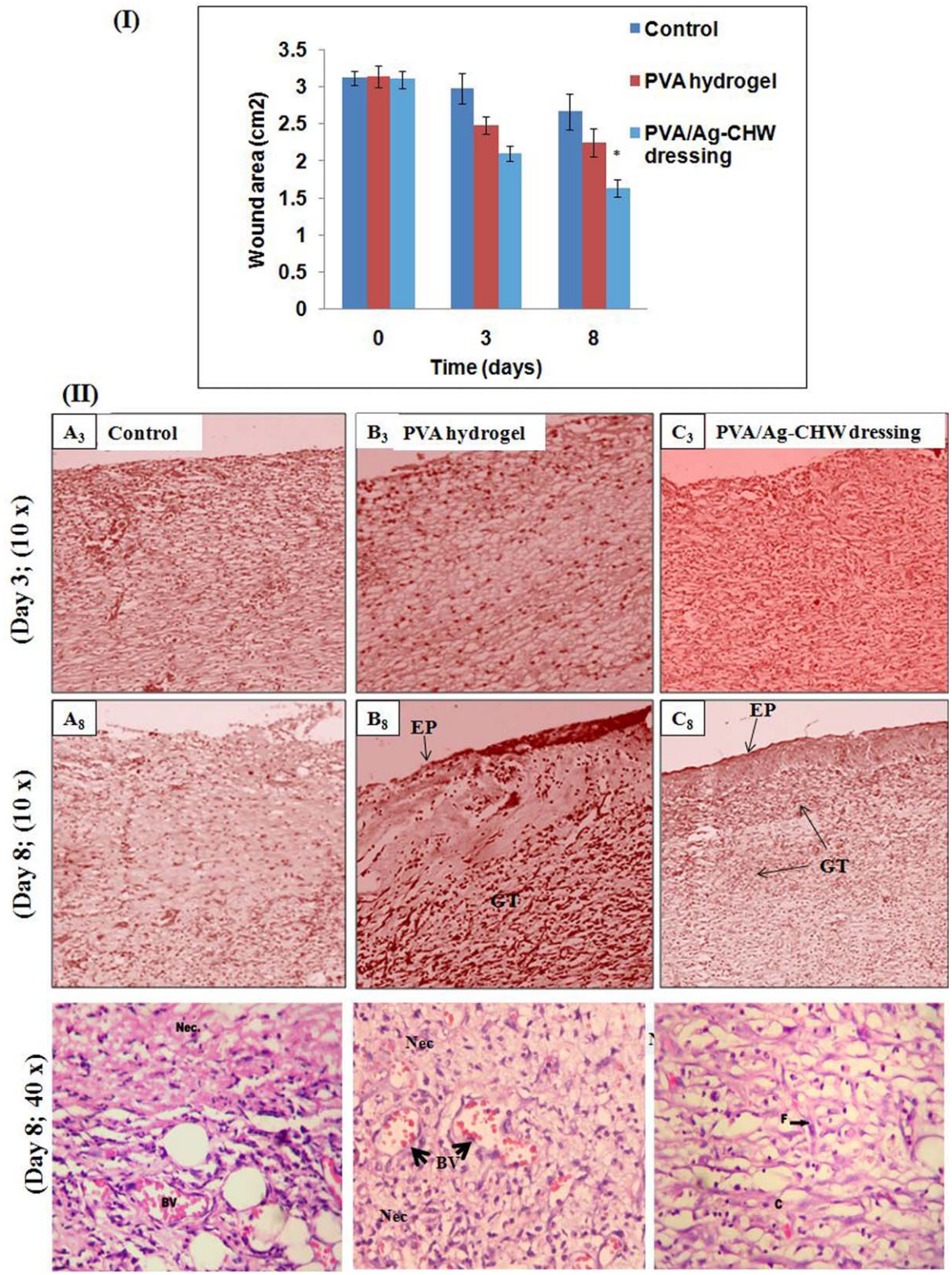

Figure 7. (I) Wound-contraction area on days 0, 3, and 8 in animal groups treated with cotton gauze, the PVA hydrogel, and the nanocomposite antimicrobial hydrogel dressing (PVA/Ag–CHW). The data were determined as means and standard deviations ($^*p < 0.05$ in comparison with cotton gauze). (II) Histological evaluation of H&E-stained skin tissue samples of (A) cotton gauze, (B) the PVA hydrogel, and (C) the PVA/Ag–CHW dressing on days 3 and 8 after wounding. BV = blood vessel; C = collagen fibrils; EP = epithelization; F = fibroblast; GT = granulation tissue; Nec = necrosis. The data were determined as means and standard deviations. [Color figure can be viewed in the online issue, which is available at wileyonlinelibrary.com.]

gauze ($2.66 \pm 0.74\,cm^2$, 15%) and PVA hydrogel ($2.24 \pm 0.6\,cm^2$, 28%) from the initial area of $3.14 \pm 0.4\,cm^2$ [Figures 6 and 7(I)].

Histological Analysis. The histopathological evaluation of the wound tissues on days 3 and 8 after the application of the controls and the hydrogel dressings are demonstrated in Figure 7(II). The inflammatory response toward the hydrogels, granulation tissue formation, collagen deposition, neoangiogenesis, and re-epithelization of the wound tissues were observed as prohealing parameters and were graded according to their response. Maximum and minimum responses were scored as $+++$ and $-$, respectively (see Table 2 in the Supporting Information).

A low-power photograph (10×) of the H&E-stained section of the control group [gauze; Figure 7(II-A_8)] showed a high inflammatory response and polymorphonuclear leucocytes infiltration on the top, whereas with a higher magnification (40×), the deeper zone of the wound bed was observed with many blood vessels, few fibroblasts, and collagen fibrils. The PVA hydrogel group [Figure 7(II-B_8)] showed a wound with the beginning of partial epithelization on the surface with a thin epidermal layer, edematous scar tissues, and scattered PMNs ($10\times$ magnification). On the other hand, at higher magnification (40×), the deeper zone of the wound bed observed with a few dilated vessels, scattered PMN infiltration, proliferated fibroblasts, and collagen formation.

The nanocomposite PVA dressing with colloidal silver (PVA/Ag–CHW) treated groups illustrated improved re-epithelization on the surface (∼49%) and scar tissue in the wound bed in comparison to the cotton gauze (∼16%) and PVA hydrogels (∼29%) with the least inflammatory response [$10\times$ magnification; Figure 7(II-C_8)]. On higher magnification (40×), the deeper zone of the wound bed was observed with only a few blood vessels, pronounced fibroblast proliferation, and collagen formation. Enhanced re-epithelization, the least inflammatory response with the progression of healing, and a higher granulation tissue formation by use of the nanocomposite dressing involved multiple factors; these included (1) the modulating effect of the AgNPs on the inflammatory mediators, that is, cytokine production; (2) an adequately moist environment; and (3) the availability of micronized chitosan around the growing tissues. In addition, the cellophane membrane prevented the excessive loss of moisture from the wound and assisted in providing the moisture requisite of the dressing. Histological analysis established the biocompatibility and safety aspect of the dressing.

Angiogenesis is another crucial factor required for the progression of healing as it ensures the availability of oxygen and vital nutrients for newly formed granulation tissues. Kapoor *et al.*[42] mentioned the presence of new blood vessel formation in the beginning of healing (first 3 days), and thereafter, it resolved with the maturation of wound; this resulted in a characteristic avascular scar. The nanocomposite dressing also helped to keep vital nutrients (growth factors, plasma proteins) in the wound milieu around the injured environment to promote the maturation of wound tissue.

An optimum concentration and uninterrupted supply of AgNPs and chitosan were required in the wound site for fibroblast proliferation activity and to elicit their best response as an antimicrobial and healing promoter, respectively;[7] beyond this value, the silver shows toxicity for cells.[21] A low level of AgNPs (4.4%) in the wound microenvironment ensured the safety of the underlying tissues/cells, that is, keratinocytes, fibroblast cells, and other nascent skin tissues. The role of the AgNPs as a modulating agent for local and systemic inflammatory mediators, such as cytokines, interleukin-10, transforming growth factor β, interleukin-6, and vascular endothelial growth factor involved in wound-healing cascade, was concentration dependent; this was achieved by the restrictive presence of AgNPs in the wound zone through our hydrogel system.[43]

CONCLUSIONS

A silver–chitosan nanocomposite hydrogel of PVA was synthesized successfully and also characterized for its physicochemical and biological properties. Chitosan was found to be an efficient stabilizing agent for the AgNPs; thereby, the multiple advantages of chitosan were incorporated into the dressing. The characterization of the PVA hydrogel ensured the practical application of the concept of reservoir-based dressing; the hydrogel showed an improved tensile strength (∼0.279 MPa) and high water retention (∼604%) along with antimicrobial properties and excellent healing potential in full-thickness wounds. By means of a histological examination of biopsied wound tissues, we observed enhanced wound healing without any undesirable inflammatory response.

ACKNOWLEDGMENTS

One of the authors (M.J.) is thankful to the Indian Council of Medical Research (India) for partial financial assistance (through a senior research fellowship). The authors are also thankful to the Indian Institute of Technology (New Delhi, India) and the All India Institute of Medical Sciences (New Delhi, India) for providing the laboratory facility and the animal facility, respectively.

REFERENCES

1. Wichterle, O.; Lim, D. *Nature* **1960**, *185*, 117.
2. Bajpai, A. K.; Shukla, S. K.; Bhanu, S.; Kankane, S. *Prog. Polym. Sci.* **2008**, *33*, 1088.
3. Chawla, P.; Srivastava, A. R.; Pandey, P.; Chawla, V. *Mini-Rev. Med. Chem.* **2014**, *14*, 154.
4. Park, K.; Shalaby, W. S. W.; Park, H. Biodegradable Hydrogels for Drug Delivery; Technomic: Lancaster, PA, **2001**; p 3.
5. Smith, T. J.; Kennedy, J. E.; Higginbotham, C. L. *J. Mech. Behav. Biomed. Mater.* **2009**, *2*, 264.
6. Sharpe, L. A.; Daily, A. M.; Horava, S. D.; Peppas, N. A. *Expert Opin. Drug Delivery* **2014**, *11*, 901.
7. Krott, M. M. C.; Munchow, M.; Periv, E.; Hebner, F.; Bozkurt, A.; Uciechowski, P.; Pallua, N.; Kroncke, K. D.; Suschek, C. C. *Free Radical Biol. Med.* **2009**, *47*, 1570.

8. Murakami, K.; Aoki, H.; Nakamura, S.; Nakamura, S. I.; Takikawa, M.; Hanzawa, M.; Kishimoto, S.; Hattori, H.; Tanaka, Y.; Kiyosawa, T.; Sato, Y.; Ishihara, M. *Biomaterials* **2010**, *31*, 3.
9. Mayet, N.; Choonara, Y. E.; Kumar, P.; Tomar, L. K.; Tyagi, C.; Du Toit, L. C.; Pillay, V. *J. Pharm. Sci.* **2014**, *103*, 2211.
10. Vlachou, E.; Chip, E.; Shale, Y. T.; Wilson, R.; Papini, N. S.; Moiemen, N. S. *Burns* **2007**, *33*, 979.
11. Widgerow, A. D. *Burns* **2010**, *36*, 965.
12. Aramwit, P.; Muangman, P.; Namviriyachote, N.; Srichana, T. *Int. J. Mol. Sci.* **2010**, *11*, 2864
13. Carter, M. J.; Tingley-Kelley, K.; Warriner, R. A. *J. Am. Acad. Dermatol.* **2010**, *63*, 668.
14. Leaper, D. L. *Int. Wound J.* **2006**, *3*, 282.
15. Greer, N.; Foman, N. A.; MacDonald, R.; Dorrian, J.; Fitzgerald, P.; Rutks, I.; Wilt, T. *J. Ann. Int. Med.* **2013**, *159*, 532.
16. Powers, J. G.; Morton, L. M.; Phillips, T. J. *Dermatol Ther.* **2013**, *26*, 197.
17. Raveendran, P.; Fu, J.; Wallen, S. L. *J. Am. Chem. Soc.* **2003**, *125*, 13940.
18. Tian, J.; Wong, K. K. Y.; Ho, C. M.; Lok, C. N.; Yu, W. Y.; Che, C. M.; Chiu, J. F.; Tam, P. K. H. *Chem. Med. Chem.* **2007**, *2*, 129.
19. Lu, Y.; Spyra, P.; Mei, Y.; Ballauff, M.; Pich, A. *Macromol. Chem. Phys.* **2007**, *208*, 254.
20. Mohan, Y. M.; Lee, K. J.; Premkumar, T.; Geckeler, K. E. *Polymer* **2007**, *48*, 158.
21. Takashi, M.; Okumura, M.; Matsuura, M.; Ueno, M.; Tokura, S.; Okamoto, Y.; Minami, S.; Fujinaga, T. *Biomaterials* **1997**, *18*, 947.
22. Phu, D. V.; Lang, V. T. K.; Lan, N. T. K.; Duy, N. N.; Chau, N. D.; Du, B. D.; Cam, B. D.; Hein, N. Q. *J. Exp. Nanosci.* **2010**, *5*, 169.
23. Twu, Y. K.; Chen, Y. W.; Shih, C. M. *Powder Technol.* **2008**, *185*, 251.
24. Jaiswal, M.; Gupta, A.; Agrawal, A. K.; Jassal, M.; Dinda, A. K.; Koul, V. *J. Biomed. Nanotechnol.* **2013**, *9*, 1495.
25. Hassan, C. M.; Peppas, N. A. *Macromolecules* **2000**, *33*, 2472.
26. Schmedlen, R. H.; Masters, K. S.; West, J. L. *Biomaterials* **2002**, *23*, 4325.
27. Vrana, N. E.; Grady, A. O.; Kay, E.; Cahill, P. A.; McGuinness, G. B. *J. Tissue Eng. Regen. Med.* **2009**, *3*, 567.
28. Okitsu, K.; Mizukoshi, Y.; Yamamoto, T. A.; Maeda, Y.; Nagata, Y. *Mater. Lett.* **2007**, *61*, 3429.
29. Jaiswal, M.; Gupta, A.; Dinda, A. K.; Koul, V. *Biomed. Mater.* **2010**, *5*, 065014.
30. Jaiswal, M.; Dinda, A. K.; Gupta, A.; Koul, V. *J. Appl. Polym. Sci.* **2015**, *132*, 42120.
31. Bhaskar, H. N.; Udupa, S. L.; Udupa, S. L. *Indian J. Physiol. Pharmacol.* **2004**, *48*, 111.
32. El-Sawy, N. M.; Abd El-Rehim, H. A.; Elbarbary, A. M.; Hegazy, E. A. *Carbohydr. Polym.* **2010**, *79*, 555.
33. Drake, P. L.; Hazelwood, K. *J. Ann. Occup. Hyg.* **2005**, *49*, 575.
34. Gupta, S.; Webster, T. J.; Sinha, A. *J. Mater. Sci. Mater. Med.* **2011**, *22*, 1763.
35. Jaiswal, M.; Ramesh, N. G.; Koul, V. *React. Funct. Polym.* **2013**, *73*, 1493.
36. Jaiswal, M.; Koul, V.; Dinda, A. K.; Mohanty, S.; Jain, K. G. *J. Biomed. Mater. Res. B* **2011**, *98*, 342.
37. Lamke, L. O.; Nilsson, G. E.; Reithner, H. L. *Burns* **1977**, *3*, 159.
38. Mbhele, Z. H.; Salemane, M. G.; Van Sittert, C. G. C. E.; Nedeljkovic, J. M.; Djokovic, V.; Luyt, A. S. *Chem. Mater.* **2003**, *15*, 5019.
39. Chou, H. L.; Wu, C. M.; Lin, F. D.; Rick, J. *AIP Adv.* **2014**, *4*, 087111.
40. Lee, S.; Tong, X.; Yang, F. *Acta Biomater.* **2014**, *10*, 4167
41. Ounsi, H. F.; Al-Shalan, T.; Salameh, Z.; Grandini, S.; Ferrari, M. *J. Endod.* **2008**, *34*, 53.
42. Kapoor, M.; Howard, R.; Hall, I.; Appleton, I. *Am. J Pathol.* **2004**, *165*, 299.
43. Liu, X.; Lee, P. Y.; Ho, C. M.; Lui, V. C.; Chen, Y.; Che, C. M.; Tam, P. K.; Wong, K. K. *Chem. Med. Chem.* **2010**, *5*, 468.